Hindawi
Geofluids
Volume 2023, Article ID 1253236, 11 pages
https://doi.org/10.1155/2023/1253236

Research Article

Study on Synchronous Response Law of Acoustic and Electrical Signals of Outburst Coal Rock under Load and Fracture

Anhu Wang,[1,2] **Liming Qiu**,[2] **Yingjie Liu**,[3] **Quan Lou**,[4] **Zuo Sun**,[3] **and Weixiang Wang**[5]

[1]*Technical Support Center for Prevention and Control of Disastrous Accidents in Metal Smelting, University of Science and Technology Beijing, Beijing 100083, China*
[2]*School of Civil and Resources Engineering, University of Science and Technology Beijing, Beijing 100083, China*
[3]*Emergency Science Research Academy, China Coal Research Institute, Beijing 100013, China*
[4]*School of Municipal and Environmental Engineering, Henan University of Urban Construction, Pingdingshan 467036, China*
[5]*BGRIMM Technology Group, No. 22, Beixing Road, Daxing District, Beijing 102628, China*

Correspondence should be addressed to Yingjie Liu; liuyingjie7777@qq.com

Received 17 May 2022; Revised 21 July 2022; Accepted 8 August 2022; Published 28 April 2023

Academic Editor: Peng Hou

A multisignal nanosecond synchronous acquisition system to measure acoustic emission (AE) and electromagnetic radiation (EMR) generated during the process of loading and failure of coal and rock samples is established. The correlation between the energy of the AE and EMR signals and the loading stress of outburst coal-rock samples was studied, and the characteristics of the AE and EMR signals during the process of loading and fracturing the outburst coal and rock samples were analyzed. The results show that (1) before the failure of the outburst coal and rock samples, the fluctuation of the AE and EMR signals is the largest, with the same rising and falling trend, and the intensity is not strictly positively correlated, with the phenomenon of low EMR when the AE intensity is high; (2) the EMR and AE deviation degree and frequency exhibit a good response to coal and rock fracturing. The correlation between EMR and stress drop is stronger than that of AE, and the AE signal is richer than the EMR signal. The results show that it is feasible to develop combined AE and EMR early warning technology to improve the early forecasting accuracy of coal and gas outbursts.

1. Introduction

Many studies at home and abroad show that the energy accumulated in coal and rock masses is released in the form of acoustic emission (AE), electromagnetic radiation (EMR), and so on [1–4]. As real-time and continuous geophysical monitoring methods, AE and EMR monitoring is widely used in structural stability monitoring, coal and gas outburst monitoring, rock burst monitoring, and other fields. With the increasing depth and intensity of coal mining in recent years, there is an increasing risk of coal and rock dynamic disasters occurring, thereby threatening the safe production of coal [5–8]. Using AE and EMR monitoring methods to achieve accurate monitoring and early warning of coal and rock dynamic disasters is very important for disaster prevention and control and is worthy of further study.

AE is a kind of elastic wave phenomenon produced by the energy released from the fracturing of solid materials. Compared with EMR monitoring of coal and rock, there have been more studies performed on AE monitoring and it is also more widely used. Zhao [9], Cao et al. [10], and Gao et al. [11] have studied the theoretical and measured AE signal characteristics from coal and gas outbursts. Liu et al. [12] focused on AE characteristics during coal seam excavation and outburst in a structural belt and revealed that the AE signal could better reflect the dynamic changes in the coal and rock. Yu and Fu [13] used a wavelet packet transform to extract the AE signal completely from the noise

during a coal and gas outburst, thereby increasing the accuracy of the early warning system.

EMR is a type of electromagnetic energy released in the process of deformation and fracture of coal and rock masses and is closely related to the loading condition, deformation, and fracture processes in the coal and rock mass. Frid [14–16], a former Soviet scholar, studied the physical and mechanical state of coal and the influence of gas on the EMR intensity of the working face. Frid reported that the increase in rock and gas outburst disasters leads to changes in the geophysical parameters of rock near the mining face and that rock and gas outbursts can be predicted by monitoring the EMR signal generated by rock fracture. Liu et al., He, and Wang et al. [17–21] proved for the first time in China that EMR is produced in the process of coal deformation and failure, the EMR signal generated in the process of fracture has low-frequency characteristics, and the frequency ranges from several hertz to several kilohertz. Thereafter, an EMR test system of electrical parameters of loaded coal rock was established, and a noncontact portable and real-time EMR monitoring instrument for predicting coal and rock dynamic disasters was developed. Moreover, a noncontact, continuous, and dynamic monitoring and early warning system for coal and rock dynamic disasters based on the combination of critical value and dynamic trends has been put forward. Pan et al. [22–24] studied the characteristics of charge induction signals in the process of coal and rock mass fracturing and applied them in the prediction of coal and rock mass dynamic disaster.

Poturayev et al. [25] performed a comparative study on AE and EMR of coal and rock under load and showed that the combined characteristics of AE and EMR can be used to monitor the stress state of the coal seams at risk of outburst near the working face. In view of the different frequency characteristics, Lou et al. [26] studied the AE and EMR variation of coal fractures under uniaxial compression and analyzed its time domain and frequency domain characteristics. Wang et al. [27] also found that AE and EMR synchronous monitoring technology to predict coal and rock dynamic disasters can solve the problem of EMR signals being susceptible to interference from underground electromagnetic fields (such as those from electromechanical sources and electrical equipment) and that the prediction accuracy of coal and rock dynamic disasters is higher.

It is clear that there are many studies on the response characteristics of AE and EMR under loading, but few studies have been performed on their synchronous response characteristics; also, these studies have not been performed at the nanosecond scale. Nanosecond synchronous acquisition is of great significance in the study of the generation mechanism of AE and EMR signals from coal and rock microfracturing. It is also important to analyze the spectrum characteristics of AE and EMR signals and obtain an AE and EMR monitoring and early warning system to predict coal and rock fracturing. Therefore, in this study, a nanosecond synchronous acquisition system of acoustic electrical signals from coal and rock under loading force was established. Furthermore, the characteristics of the synchronous AE and EMR response during the process of loading and fracturing of coal and rock samples were systematically studied.

2. Experimental System and Scheme

2.1. Synchronous Acquisition Experimental System. In this study, the simultaneous acquisition of acoustic and electrical signals of outburst coal rock under uniaxial compression force was obtained in the research group of Safety Rheology Mutation, University of Science and Technology Beijing. The experimental system includes a loading control system, a synchronous acoustic and electrical data acquisition system, and an electromagnetic shielding system. The details are as follows:

(1) Loading control system: this is mainly used for the uniaxial compression test of the coal and rock. Loading control is carried out on a YAW-600 microcomputer-controlled electrohydraulic servo rock testing machine, as shown in Figure 1. The entire process of uniaxial compression stress–strain curve of coal and rock can be measured in the compression process of coal and rock samples, and there are three control modes of test stress (stress, load), deformation (axial strain, radial strain), and displacement (compression rate). The performance indexes of the testing machine are listed in Table 1

(2) Synchronous acquisition system: this system includes a high-speed data acquisition instrument (as shown in Figure 2) and a data storage and analysis computer. The principle and connection diagram of the AE and EMR signal acquisition are shown in Figure 3. The high-speed data acquisition instrument shown in the figure consists of 12 data acquisition channels and the synchronous AE and EMR signal trigger. The acquisition frequency of each channel is 10 MHz (interval 100 nanoseconds), the A/D conversion accuracy is 16 bits, the input signal voltage range is ±5 V, and the synchronous acquisition error of the AE, EMR, and load signals is ≤1 ms. The response frequency of the AE sensor used in this experiment is in the range of 50–400 kHz; the preamplifier magnification is 20, 40, and 60 dB adjustable; the built-in filter frequency band is 20 kHz–1.5 MHz; the input impedance is >10; the output impedance is 50. The EMR sensor adopts the loop receiving field antenna SAS-560 whose frequency range is 20 Hz–2 MHz, and the amplification rate of the EMR preamplifier is 80 dB

(3) EMR signals exist widely in daily life, and all types of instruments and electrical appliances used in the laboratory can produce EMR signals. To eliminate the influence of these interference signals on the experiment and ensure the accuracy of the experimental data, the servo press was placed in the GP1 electromagnetic shielding room. The shell of the shielding room was made of 2 mm thick high-quality cold-

(a) YAW-600 microcomputer-controlled loading system (b) EMR shielding room

Figure 1: Experimental equipment.

Table 1: Performance index of the testing machine.

Category	Parameter value	Category	Parameter value
Maximum test force	600 kN	Stiffness K	≥5000 kN mm^{-1}
Piston stroke	≥60 mm	Relative error of test force	±1%
Measurement range	0–60 mm	Test force sensing element	Pressure sensor
Experimental resolution	3 N	Test force resolution	1/200000%fs
Displacement resolution	0.3 μm	Resolution	1/200000%fsmm
Relative error	±0.5%	Clear width of test space	300 mm

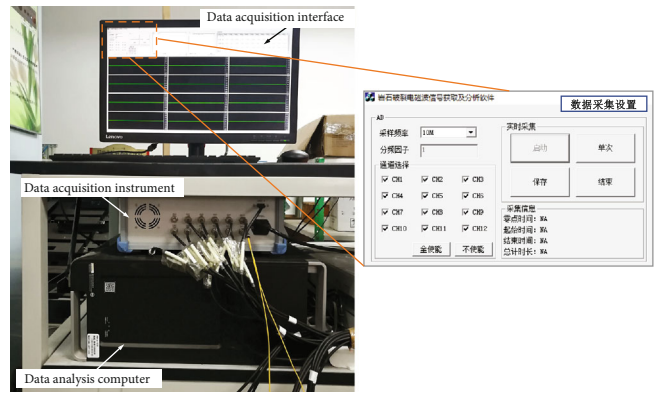

Figure 2: Synchronous acquisition and analysis system of AE and EMR signal data.

rolled steel plate. The shielding effectiveness indexes of the shielding room are as follows: 14 kHz ≥ 75 dB, 100 kHz ≥ 95 dB, 200 kHz ≥ 100 dB, and 50 − 100 MHz ≥ 110 dB. In the experiment, the AE and EMR sensors were placed in the shielding room and the acquisition instrument was placed outside the shielding room. A connecting line connected the sensor and the acquisition instrument through a waveguide

2.2. Sample Preparation and Experimental Scheme

(1) Sample preparation: the coal and rock samples used in this experiment were collected from the Jinjia coal mine, a typical outburst mine in the Panjiang Mining Area. The type of coal is fat coal, with 10.24% volatile, 15.63% ash, and 2.58% moisture measured in the laboratory. The strength of the coal samples was low; thus, it was difficult to prepare raw coal samples. Therefore, the coal samples in this experiment were all in the form of briquettes. The specific production process of briquette is as follows: (1) use hammers, crushers, etc. to crush large pieces of coal into smaller ones; (2) the pulverized coal with a particle size of 0~1 mm and 1~3 mm shall be sieved with a sieve and mixed according to the proportion of 76% and 24%; (3) the mixed pulverized coal is evenly

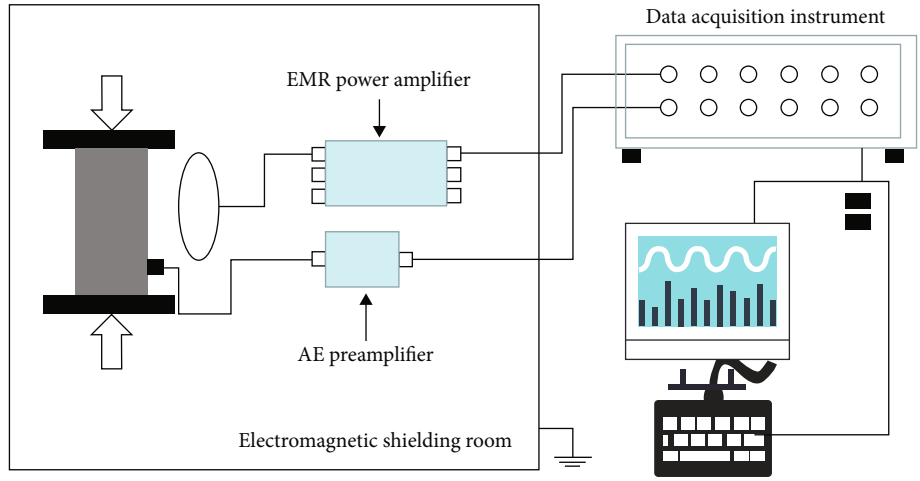

Figure 3: Schematic illustration of the synchronous acquisition experimental system.

mixed with 20% sodium humate and placed in the briquette mold, and the servo press is used to press the briquette sample to ensure that the peak pressure of 30 kN is applied for about 15 min to make the pressing range 50 mm × 100 mm standard coal sample; (4) after the coal sample is pressed, it is put into the drying oven for drying and then sealed with fresh-keeping film. The rock samples used in the experiment were fine sandstones obtained from the outburst coal seam roof. Detailed statistics are presented in Table 2

(2) Experimental steps: this experiment was used to study the synchronous response characteristics of the EMR and AE signals measured in the process of loading deformation and fracture of the coal and rock samples. The detailed experimental steps are as follows:

(1) A vernier caliper is used to measure the size of the coal forming rock sample; then, the development of cracks and textures on the sample surface is carefully observed and recorded

(2) All types of experimental instruments are connected according to the requirements; the status of instruments is checked, and preliminary debugging is carried out

(3) The EMR receiving antenna is connected well, and the AE sensor is bonded with the sample surface with a specific coupling agent

(4) It is then ensured that the instrument, transmission line, and shielding system are well-grounded; the press testing machine system is then started, and the control mode and acquisition parameters are set according to the experimental requirements; environmental noise monitoring is conducted for a period of time, and the threshold value of each channel is debugged and set

(5) The continuous uniaxial loading mode is adopted for m6–m9 briquette, and the axial compression loading rate is 30 N s^{-1}. The uniaxial cyclic loading mode is adopted for the test of the M11 briquette, and two loading cycles are adopted until the loading failure. The starting point of the cycle is 1.5 kN, the initial force is 500 N, and the axial compression loading rate is 5 N s^{-1}. The displacement-controlled loading mode is adopted for the Y1–Y4 rock samples, and the loading rate is 2 μM s^{-1}

(6) At the end of the experiment, data collection first stops, and then, the testing machine is turned off; then, the EMR and AE data are saved in turn

(3) Data processing method: the characteristics of the AE and EMR are described in terms of the characteristic parameters of AE and EMR, namely, data amplitude E, energy Em, and ring count (pulse, etc.) N. The specific data processing process is as follows:

(1) By using the full waveform processing software of the acquisition instrument, the threshold value of the effective signal and interference signal is selected

(2) The data are read through the MATLAB software. Based on the amplitude characteristics of the entire process, the appropriate threshold voltage is selected to filter out the interference signals from the original AE and EMR signals, and the useful signal is extracted

(3) According to the threshold voltage and waveform identification time of the AE signal, the AE event is determined, and the parameters of the AE and EM signals, such as amplitude, duration, ringing count, and energy, are obtained

Table 2: Actual size of experimental coal and rock sample.

Sample number	Sample type	Diameter (mm)	Height (mm)	Weight (g)	Remarks
M6	Coal	50.8	96.9	269.59	
M7	Coal	52	95.3	276.04	
M8	Coal	50.2	94	263.98	
M9	Coal	52.3	99.4	287.04	
M10	Coal	52.1	101	285.35	Measurement of synchronous response characteristics of acoustic and electrical signals
M11	Coal	52	101.2	285.48	
Y1	Rock	51.4	100.6	511.41	
Y2	Rock	52.7	96.3	510.82	
Y3	Rock	50.6	100.5	492.21	
Y4	Rock	51.9	102.4	501.23	

3. Synchronous AE and EMR Response from Coal and Rock Fracturing

3.1. Results of Synchronous AE and EMR Testing of Coal and Rock Fracturing. The stress–strain curves and acoustic signal data of 10 outburst coal-rock samples were measured through the simultaneous acquisition of acoustic and electrical signals of the coal and rock samples under load from the test system. Among the 10 samples, the acoustic and electrical signals collected from briquette samples were generally weak, and those from the rock samples under the process of loading and fracture were better. In this study, four groups of coal and rock samples (M6, M10, Y1, and Y3) with good acoustic and electrical data acquisition effects were selected for analysis.

Figure 4 exhibits that the force control rate of the sample is 30 N s^{-1}, the instability time is 134 s, and the peak stress is 2.0 MPa. The changes of AE, EMR, and stress of the coal samples with time are as follows: at the initial stage of loading, with the gradual increase in pressure, there is no obvious EMR and AE signal. With the further increase in the pressure, a small amount of AE and EMR signals appear. When the load continues to increase, the deformation of the sample becomes serious, the stress curve suddenly drops to a lower value, and the sample gets seriously broken. At this time point of sudden pressure drop, the AE and EMR signals increase sharply. In general, the AE signal increases earlier than the EMR signal.

Figure 5 shows that the initial force of the sample is 500 N, the loading rate is 5 N s^{-1}, the peak stress is 1.7 MPa, and the instability time is 1239 s. In the first cyclic loading process, the AE and EMR signals of the sample are generally weak and in a relatively stable state. At 524 s, the first cyclic loading peak appears, while the AE exhibits a small peak; however, the EMR remains stable. At this time, tiny cracks appear in the coal body. At 1211 s, the maximum wave peaks of the AE and EMR signals are 4 V and 0.17 V, respectively.

Figure 6 demonstrates that for the Y1 rock sample, the peak stress of the loading rate is 100 MPa, and the instability time is 500 s. The figure illustrates that at the initial stage of loading, the AE and EMR signals are at a relatively low level and change smoothly. At 80 and 160 s, owing to the microfracturing in the rock mass, the AE signal exhibits a small peak, and the EMR signal shows no obvious change. With the increase in the stress, a series of peaks appear in the AE at around 300 s, while the EMR shows a small peak. After reaching the peak stress at 430 s, the stress curve continuously shows a stress drop. In the process of the stress drop, along with the large increase in the AE and EMR values, the AE appears to have a stepped upward trend, and the maximum peak value is 3 V at 475 s. The peak value of the EMR signal is 0.18 v at 497 s. Clearly, the fluctuation of the AE and EMR signals is the largest in the preinstability stage of the rock, showing a trend of rising and falling at the same time. It is consistent in time, but not strictly positive in intensity. Thus, the phenomenon that the EMR is low when the AE intensity is high and vice versa is observed.

Figure 7 shows that the peak stress of the Y3 rock sample is 85 MPa and the instability time is 670 s. The figure clearly illustrates that at the initial stage of stress rise, the AE and EMR have no obvious change. At about 468 s, the rock stress reaches the peak value, and then, the stress drops continuously. At the same time, the system monitors a large number of AE and EMR signals, the peak value of the AE is 4 V, and the peak value of the EMR is 0.46 V. During the loading process, the AE and EMR show the same rising and falling trend, which is consistent in time and not strictly positively correlated in intensity. The phenomenon of low EMR occurs when the AE intensity is high, and vice versa.

3.2. Synchronous Response Characteristics of Acoustic and Electrical Signals. Through in-depth analysis of the synchronous acquisition results of the AE and EMR signals in the loading and fracture processes of the M6, M10, Y1, and Y3 samples, it can be concluded that the synchronous acoustic electrical response of the outburst coal-rock samples shows the following characteristics:

(1) In general, the AE signal and EMR signal are positively correlated with the loading stress of the coal and rock samples. In other words, in the loading process of the coal and rock samples, with the increase in the loading stress, the AE and EMR values increase. The synchronization of EMR and AE is related to the stress state of coal and rock. In the elastoplastic stage, the synchronization is poor,

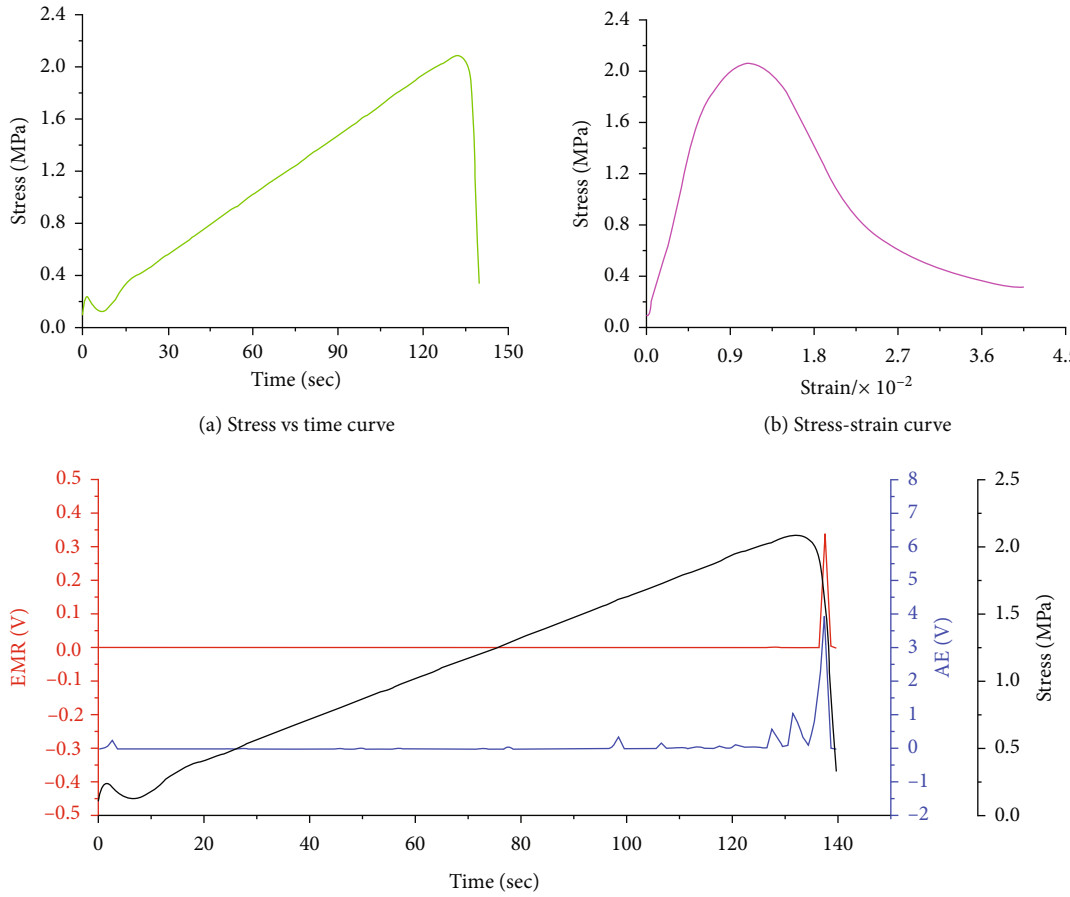

(a) Stress vs time curve

(b) Stress-strain curve

Figure 4: EMR, AE, and stress change of the M6 coal sample.

but in the crushing stage, the synchronization is better. The reason for this phenomenon is that in the elastoplastic stage, there are primary cracks in the sample, the fracture energy is small, and the response of EMR to these small energy releases is not obvious. However, AE has a good response to these small energy elastic wave releases. In the crushing stage, the internal fracture energy of coal and rock samples is large, and the response of EMR and AE to fracture events is increased. Therefore, the AE and EMR values are reliable indicators for monitoring their stress state of coal and rock masses

(2) Irrespective of the type of coal sample or rock sample, the intensity of the AE signal and the EMR signal and the number of events increase sharply in the coal rock fracture stage before and after the peak stress. For example, during the period from 120 s to the loading failure stage, the EMR value of the M6 coal sample reaches 0.34 V at 137.5 s, while the EMR signal is hardly detected before that. During this period, the increase in the AE is more obvious; the maximum value reaches 3.97 V, which is far greater than the base value of the AE signal at the early stage of loading, and the frequency of the AE signal after 120 s is 6, which is far greater than the abnormal number in the first 120 s. Similarly, in the entire process of loading and fracture of the Y1 rock sample, the base value of the EMR is almost zero before the stress reaches the peak value at 450 s, and the internal fracture in the rock mass intensifies at 450 s. Further, the EMR intensity and abnormal frequency increase sharply after 450 s; the maximum value is 0.16 V, and the frequency is 5, which is far greater than the previous value. The AE frequency also abnormally increases at this stage. The intensity and frequency of the EMR and AE signals of the Y3 rock sample increase significantly beyond 480 s. Therefore, the deviation degree and frequency of the EMR and AE signals show a good response to coal and rock fracturing

(3) The AE and EMR signals have good consistency in time and can be considered to be caused by the same fractures in the sample, which is consistent with the results of previous studies [28–32]. However, noteworthily, the AE and EMR signal strengths are not strictly positively correlated and show some differences. The specific performance is that there is high-intensity AE accompanied by low-intensity EMR, and vice versa, which is most obvious in the Y1 and Y3 samples. The number of events of

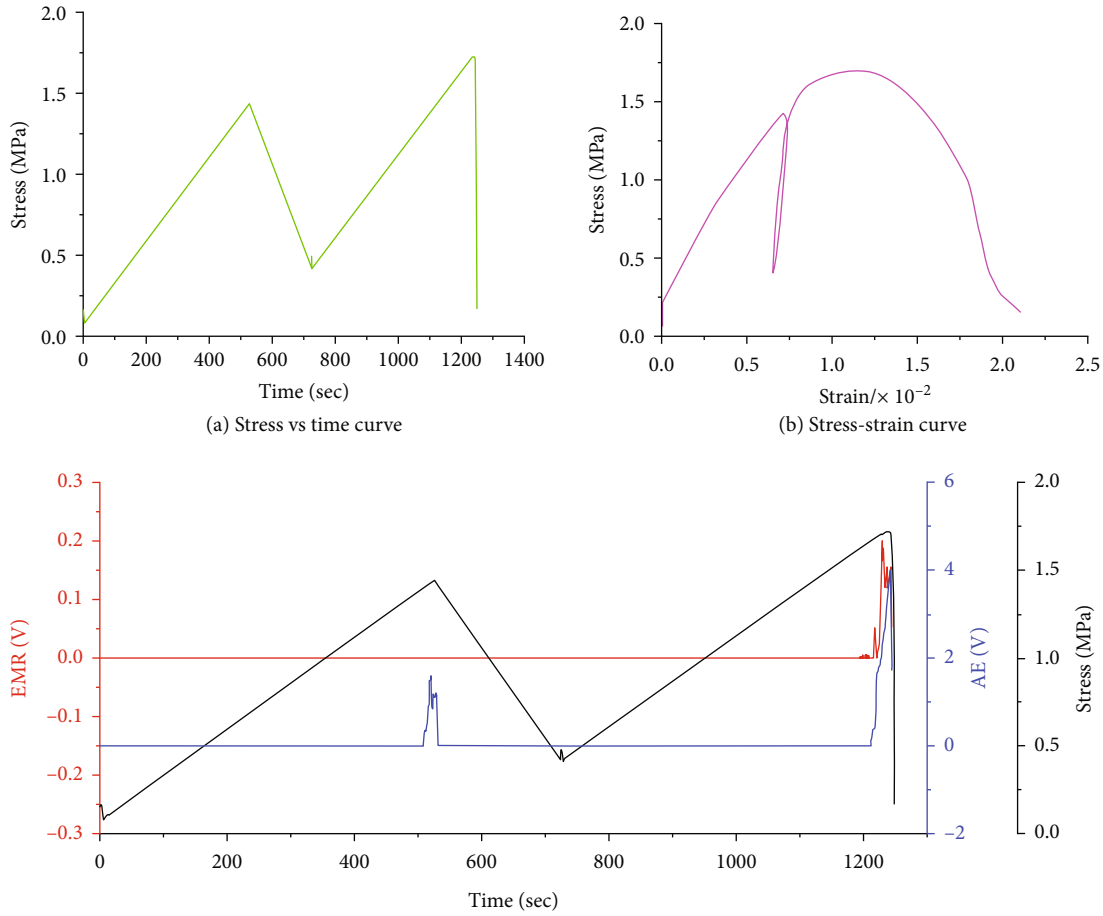

Figure 5: EMR, AE, and stress change of the M10 coal sample.

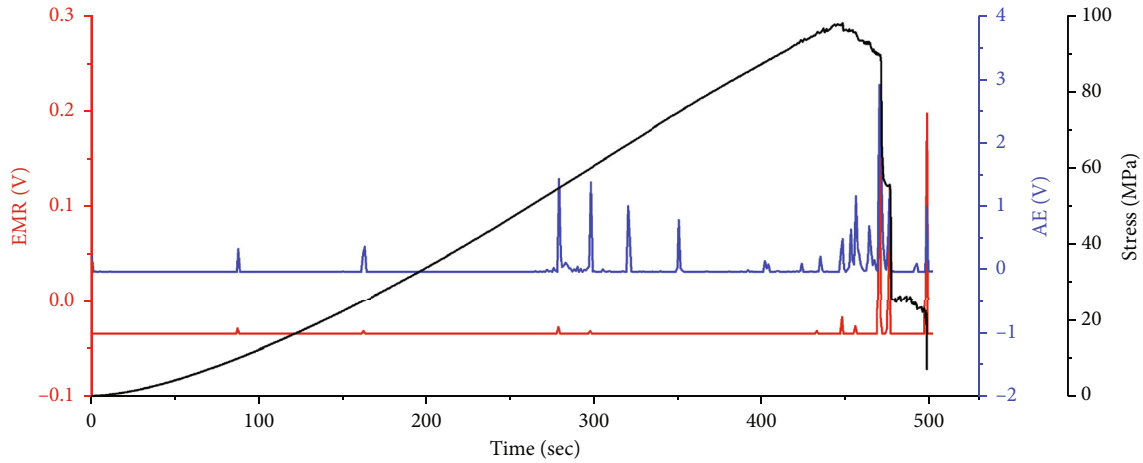

Figure 6: EMR, AE, and stress change of the Y1 rock sample.

acoustic and electrical signals of the Y1 and Y3 samples was counted, and the results are shown in Figure 8. Clearly, the number of AE events of the Y1 and Y3 samples is much larger than that of the EMR events. This indicates that the EMR signal is accompanied by the AE signal and stress drop, while the AE signal mostly appears alone

3.3. Correlation between Acoustic and Electrical Signals and Stress Drop. During the loading process of the Y1 and Y3 samples, the relationship between the acoustic electrical signal and the stress drop is obvious. To analyze the correlation between the acoustic electrical signal and the stress drop during the loading and fracture process of the coal and rock, the AE count, EMR count, and the stress drop over 1 s were

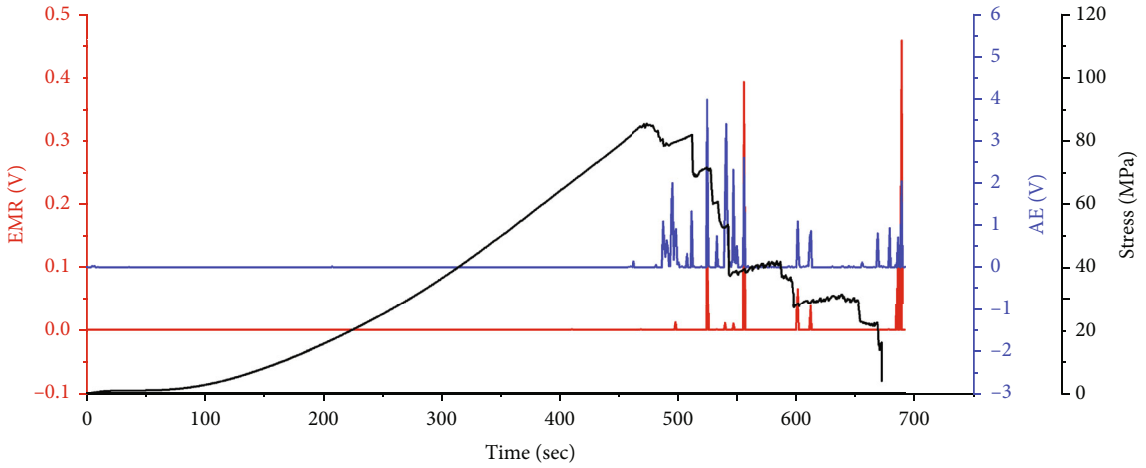

Figure 7: EMR, AE, and stress change of the Y3 rock sample.

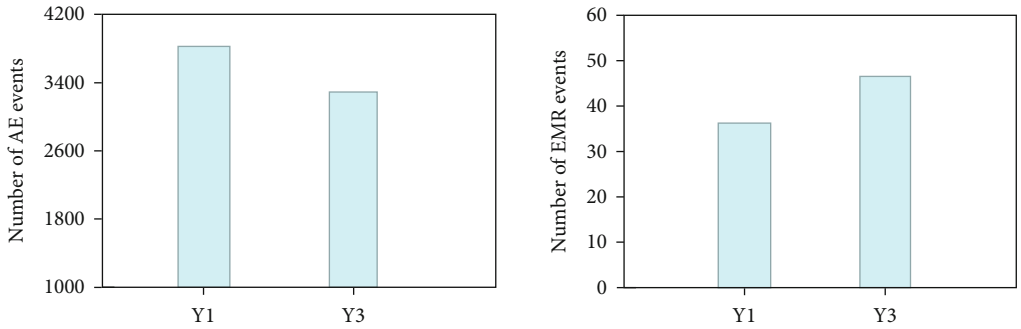

Figure 8: Comparison of the AE and EMR events of the outburst coal-rock samples.

investigated and summed up, respectively, and then, the cumulative processing was carried out.

To quantitatively analyze the consistency of AE, EMR, and stress drop during the process of load failure of an outburst coal-rock mass, the EMR count, the AE count, and the stress drop of the Y1 and Y3 samples, as well as their cumulative values, were analyzed. It is assumed that there are two sequences $x(x_1, x_2, \cdots, x_n)$ and $y(y_1, y_2, \cdots, y_n)$ of length N, and the correlation coefficient r_{xy} among them can be expressed as follows:

$$r_{xy} = \frac{\sum_{i=1}^{n}(x_i\text{-}\bar{x})(y_i\text{-}\bar{y})}{\sqrt{\sum_{i=1}^{n}(x_i\text{-}\bar{x})^2}\sqrt{\sum_{i=1}^{n}(y_i\text{-}\bar{y})^2}}. \quad (1)$$

Based on formula (1), the correlation coefficients of EMR count, AE count, cumulative EMR count, cumulative AE count, and stress drop were calculated. The results are presented in Table 3, which summarizes the following points:

(1) The correlation coefficient between the index cumulative values of each test coal sample is greater than that between the index values. From the index value to the index cumulative value, the correlation coefficients between EMR count and load drop, AE count and load drop, and AE count and EMR count exhibit an increase of 5.39% (0.89 → 0.938), 49.71% (0.511 → 0.765), and 59.35% (0.4895 → 0.78), respectively

(2) Compared to AE counting, the correlation coefficient between EMR counting and stress drop is higher. The correlation coefficient between the EMR and stress drop is 0.89, and the correlation coefficient between the AE and the stress drop is 0.511. Therefore, there is a higher correlation coefficient between the EMR and the stress drop. The correlation coefficients of AE count and stress drop and AE count and EMR count are roughly the same, which are 0.511 and 0.4895, respectively

3.4. Consistency and Difference Analysis of Acoustic and Electrical Signals. The experimental results show that the AE and EMR signals have good consistency in time during the process of outburst coal and rock fracture; the signals can be considered to be caused by the same fractures in the sample. However, the intensity of the AE and EMR signals is not strictly positively correlated and there are some differences. Compared with AE, there is a better correlation between EMR and load drop. The causes of these two phenomena are discussed as follows.

Table 3: Correlation coefficient among EMR, AE, and stress drop.

Sample number	EMR and stress drop	EMR cumulative and stress drop	AE and stress drop	AE cumulative and stress drop	EMR and AE number	EMR and AE cumulative number
Y1	0.865	0.892	0.568	0.705	0.493	0.768
Y3	0.915	0.984	0.454	0.825	0.486	0.792
Average	0.89	0.938	0.511	0.765	0.4895	0.78

3.4.1. Consistency Analysis. In this study, the stress drop in the Y1 and Y3 coal rock samples during the process of uniaxial compression and expansion fracture was found to be closely related to the generation of the EMR signal, which is consistent with the results from previous studies [33, 34]. Noteworthily, the stress drop is the external manifestation of the influence of crack evolution on the mechanical properties of the specimen. It is the process of stress redistribution and energy release caused by the local concentrated stress in the specimen exceeding the material bearing limit. Therefore, the stress drop can be considered a local stress transient phenomenon [35, 36]. In the process of crack nucleation, propagation, aggregation, and penetration, the strain and stress at the crack tip suddenly increase and decrease in a short time, which leads to the electric dipole transient at the crack tip and excitation of the EMR. Clearly, the entire process of coal and rock failure is accompanied by stress transients; however, the stress transients of different crack sizes and development stages correspond to different strengths.

Stress is the most basic and important factor affecting EMR and AE generation in granular coal and rock masses with well-developed pores and fissures [37–39]. As a driving force, the external disturbance stress causes uneven stress distribution in the coal and rock mass and makes the weak structural plane vulnerable to crack evolution to redistribute the stress, release energy, and produce stress transients. The crack evolution further leads to the evolution of a new weak structural plane driven by the external disturbance stress, until the entire sample finally loses its bearing capacity. In this process, EMR and AE are excited by stress transients. Therefore, high external disturbance stress indicates a high probability of EMR and AE [40–42], which is the fundamental reason for the good consistency of acoustic and electrical signals in time.

3.4.2. Difference Analysis. The experimental results exhibit the existence of some differences in the values of AE and EMR in the process of coal and rock fracture. Specifically, the correlation between EMR and stress drop is stronger than that of AE, and the AE signal is richer than the EMR signal. The reasons are as follows [43, 44]: AE has a high signal-to-noise ratio and is very sensitive to the release of elastic wave energy during the process of loading and fracture of coal and rock samples, which leads to the AE signal being richer than the EMR signal. Moreover, the generation of EMR is related to the stress concentration, EMR signals will be generated only when the stress concentration reaches a certain threshold, while the threshold of AE signals is relatively lower, which is the reason why the AE signal is richer than the EMR signal. Moreover, although AE is sensitive to the release of elastic wave energy, for the coal samples with primary and secondary fractures, the AE signal strength depends not only on the energy of the elastic wave released by the fractures but also on the propagation path of the elastic waves in the sample [45–47]. With increasing micro- and macrocracks in the sample, the propagation of elastic waves in the sample becomes more complex, and the attenuation characteristics change significantly compared to those at the initial stage of loading. Furthermore, the fixed position of the AE sensor causes the signal strength and frequency received by a single AE probe to change significantly compared to the AE source [48, 49]. At the later stage of loading, under the action of severe cracking, the AE sensor even falls off, or the coal attached to the sensor peels off from the main body of the sample. These results lead to the incomplete response energy of AE to fracture, in particular, the large postpeak fracture, which is directly proportional to the fracture strength, further reducing the correlation between AE and stress drop.

4. Conclusions

Using a synchronous acquisition system to measure acoustic electrical signals from outburst coal and rock under loading, the synchronous acquisition, storage, and analysis of EMR, AE, and load signal were successfully achieved. The synchronous response characteristics of AE and EMR signals during the process of coal and rock sample fracturing were compared and studied. The main conclusions are as follows:

(1) A synchronous AE and EMR acquisition system is built with a sampling frequency set at 10 MHz, which achieves the nanosecond synchronous acquisition of AE and EMR data during the process of loading and fracturing outburst coal and rock samples. The experimental data show that the outburst coal and rock samples produce AE and EMR signals during the process of fracturing, and the AE and EMR signals are positively correlated with the loading stress of the coal and rock samples. The AE intensity and EMR intensity are reliable indicators for monitoring the stress state of a coal and rock mass

(2) The AE and EMR signals synchronously collected in the experiment are consistent in time. For the same fracture event in the loading process of the coal and rock mass, the AE and EMR exhibit a good

response. The AE and EMR signal intensity are not strictly positively correlated and exhibit the phenomenon of low EMR when the intensity of AE is high

(3) Irrespective of the type of coal or rock sample, when the sample enters into the yield stage in the loading process, the AE and EMR signals show a cliff-like growth. In this stage, the relative base values of the EMR emission and the AE increase significantly, and the number of events (frequency) increases significantly. The correlation coefficient between EMR and stress drop is stronger than that between AE and stress drop. The AE signal is richer than the EMR signal

Data Availability

The data used to support the findings of this study are included within the article.

Conflicts of Interest

The authors declare that they have no conflicts of interest.

Acknowledgments

This work was financially supported by the China Postdoctoral Science Foundation (Grant No. 2020M680490), the Fundamental Research Funds for the Central Universities (Grant No. FRF-TP-22-054A1), the State Key Research Development Program of China (Grant No. 2016YFC0801408), and China Coal Technology & Engineering Group Co., Ltd. (Grant No. 2019-2-ZD003). The authors would like to express their gratitude to all the agencies for funding this research.

References

[1] G. Wen, H. Yang, and Y. Zou, "Theoretical analysis of characteristics of acoustic emission in rock failure based on statistical damage mechanics," *Journal of Coal Science and Engineering (China)*, vol. 15, no. 3, pp. 237–242, 2009.

[2] Y. Zhao, H. Zhou, J. Zhong, and D. Liu, "Study on the relation between damage and permeability of sandstone at depth under cyclic loading," *International Journal of Coal Science & Technology*, vol. 6, no. 4, pp. 479–492, 2019.

[3] X. Li, Z. Cao, and Y. Xu, "Characteristics and trends of coal mine safety development," *Energy Sources, Part A: Recovery, Utilization, and Environmental Effects*, vol. 42, pp. 1–14, 2020.

[4] X. Li, S. Chen, E. Wang, and Z. Li, "Rockburst mechanism in coal rock with structural surface and the microseismic (MS) and electromagnetic radiation (EMR) response," *Engineering Failure Analysis*, vol. 124, article 105396, 2021.

[5] X. He, X. Liu, D. Song, and B. Nie, "Effect of microstructure on electrical property of coal surface," *Applied Surface Science*, vol. 483, pp. 713–720, 2019.

[6] X. Liu, D. Song, X. He, Z. Wang, M. Zeng, and L. Wang, "Quantitative analysis of coal nanopore characteristics using atomic force microscopy," *Powder Technology*, vol. 346, pp. 332–340, 2019.

[7] F. Du, K. Wang, X. Zhang, C. Xin, L. Shu, and G. Wang, "Experimental study of coal-gas outburst: insights from coal-rock structure, gas pressure and adsorptivity," *Natural Resources Research*, vol. 29, no. 4, pp. 2481–2493, 2020.

[8] K. Wang and F. Du, "Coal-gas compound dynamic disasters in China: a review," *Process Safety and Environmental Protection*, vol. 133, pp. 1–17, 2020.

[9] H. Zhao, *Theoretical and experimental study on unstable failure and AE characteristic of coal contained gas, [Ph.D. thesis]*, Chongqing University, Chongqing, China, 2009.

[10] S. Cao, Y. Liu, and L. Zhang, "Comprehensive analysis on acoustic emission characteristics of deformation and failure of outburst coal," *Journal of rock mechanics and engineering*, vol. S1, pp. 2794–2799, 2007.

[11] B. Gao, H. Li, H. Li, R. Yuan, and Y. Liu, "Current situation of the study on acoustic emission and microseismic monitoring of coupling dynamic catastrophe for gas-filled coal-rock," *Progress in Geophysics*, vol. 29, no. 2, pp. 689–697, 2014.

[12] S. Liu, X. Li, D. Wang, and D. Zhang, "Experimental study on temperature response of different ranks of coal to liquid nitrogen soaking," *Natural Resources Research*, vol. 30, no. 2, pp. 1467–1480, 2021.

[13] H. Yu and X. Fu, "Application of wavelet packet transform in prediction of coal and gas outburst," *Journal of Heilongjiang University of science and technology*, vol. 5, pp. 279–281, 2006.

[14] V. Frid, "Electromagnetic radiation method water-infusion control in rockburst-prone strata," *Journal of Applied Geophysics*, vol. 43, no. 1, pp. 5–13, 2000.

[15] V. Frid, "Calculation of electromagnetic radiation criterion for rockburst hazard forecast in coal mines," *Pure and Applied Geophysics*, vol. 158, no. 5, pp. 931–944, 2001.

[16] V. Frid and K. Vozoff, "Electromagnetic radiation induced by mining rock failure," *International Journal of Coal Geology*, vol. 64, no. 1-2, pp. 57–65, 2005.

[17] M. Liu, X. He, and D. Li, "Experimental study on Kaiser effect of fracture electromagnetic radiation," *Journal of Jiaozuo University of mining and technology*, vol. 4, pp. 89–96, 1995.

[18] X. He, *Rheological Electromagnetic Dynamics of Coal and Rock*, Science Press, Beijing, China, 2003.

[19] E. Wang, X. He, B. Nie, and Z. Liu, "Principle of predicting coal and gas outburst using electromagnetic emission," *Journal of China University of Mining and Technology*, vol. 29, no. 3, pp. 225–229, 2000.

[20] E. Wang, X. He, L. Dou, S. Zhou, and B. Nie, "Electromagnetic radiation characteristics of coal and rocks during excavation in coal mine and their application," *Chinese Journal of Geophysics*, vol. 48, no. 1, pp. 216–221, 2005.

[21] E. Wang, X. He, J. Wei, B. Nie, and D. Song, "Electromagnetic emission graded warning model and its applications against coal rock dynamic collapses," *International Journal of Rock Mechanics and Mining Sciences*, vol. 48, no. 4, pp. 556–564, 2011.

[22] Y. Zhao, Y. Pan, G. Li, W. Ren, and H. Luo, "Measuring of the charge-induced signal of rock during the deformation and fracture process," *Journal of disaster prevention and mitigation engineering*, vol. 30, no. 3, pp. 252–256, 2000.

[23] Y. Pan, H. Luo, X. Xiao, Y. Zhao, and Z. Li, "Experimental study on mechanical charge induction law of coal containing gas under triaxial compression," *Journal of China Coal Society*, vol. 37, no. 6, pp. 918–922, 2012.

[24] Z. Tang, Y. Pan, Z. Li, H. Yan, G. Li, and Y. Zhao, "Application of charge detection of coal-rock in the dynamic disaster

prediction," *Chinese Journal of geological disasters and prevention*, vol. 21, no. 3, pp. 109–112, 2010.

[25] V. Poturayev, A. Bulat, and V. Khokholev, "Combined detection of electromagnetic and acoustic emission associated with rock failure," *Transactions (Doklady) of the USSR Academy of Sciences: Earth Science Sections*, vol. 5, pp. 86–89, 1989.

[26] X. Q. He, C. Zhou, D. Z. Song et al., "Mechanism and monitoring and early warning technology for rockburst in coal mines," *International Journal of Minerals, Metallurgy and Materials*, vol. 28, pp. 1097–1111, 2021.

[27] E. Wang, X. Liu, X. He, and Z. Li, "Acoustic emission and electromagnetic radiation synchronized monitoring technology and early-warning application for coal and rock dynamic disaster," *Journal of China University of Mining and Technology*, vol. 47, no. 5, pp. 942–948, 2018.

[28] D. Song, E. Wang, Z. Li, J. Liu, and W. Xu, "Energy dissipation of coal and rock during damage and failure process based on EMR," *International Journal of Mining Science and Technology*, vol. 25, no. 5, pp. 787–795, 2015.

[29] S. He, D. Song, Z. Li et al., "Precursor of spatio-temporal evolution law of ms and AE activities for rock burst warning in steeply inclined and extremely thick coal seams under caving mining conditions," *Rock Mechanics and Rock Engineering*, vol. 52, no. 7, pp. 2415–2435, 2019.

[30] Q. Lou, *Theory and experimental study on electromagnetic radiation location of coal and rock failure*, China University of mining and Technology (Beijing), Beijing, China, 2019.

[31] G. Niccolini, J. Xu, A. Manuello, G. Lacidogna, and A. Carpinteri, "Onset time determination of acoustic and electromagnetic emission during rock fracture," *Progress in Electromagnetics Research Letters*, vol. 35, pp. 51–62, 2012.

[32] A. Carpinteri, G. Lacidogna, O. Borla, A. Manuello, and G. Niccolini, "Electromagnetic and neutron emissions from brittle rocks failure: experimental evidence and geological implications," *Sadhana*, vol. 37, no. 1, pp. 59–78, 2012.

[33] T. Zhu, J. Zhou, and H. Wang, "Electromagnetic emissions during dilating fracture of a rock," *Journal of Asian Earth Sciences*, vol. 73, pp. 252–262, 2013.

[34] A. Takeuchi and H. Nagahama, "Voltage changes induced by stick-slip of granites," *Geophysical Research Letters*, vol. 28, no. 17, pp. 3365–3368, 2001.

[35] K. Fukui, S. Okubo, and T. Terashima, "Electromagnetic radiation from rock during uniaxial compression testing: the effects of rock characteristics and test conditions," *Rock Mechanics and Rock Engineering*, vol. 38, no. 5, pp. 411–423, 2005.

[36] Q. Lou, D. Song, X. He et al., "Correlations between acoustic and electromagnetic emissions and stress drop induced by burst-prone coal and rock fracture," *Safety Science*, vol. 115, pp. 310–319, 2019.

[37] H. Wang, S. Guo, Y. Xie, H. Zhao, H. Wang, and W. Wang, "Study on competitive adsorption characteristics of $CO/CO_2/CH_4$ multi-component low concentration gases in coal," *Energy Sources Part A Recovery Utilization and Environmental Effects*, vol. 42, pp. 1–15, 2020.

[38] H. Wang, B. Tan, and X. Zhang, "Research on the technology of detection and risk assessment of fire areas in gangue hills," *Environmental Science and Pollution Research*, vol. 27, no. 31, pp. 38776–38787, 2020.

[39] F. Du and K. Wang, "Unstable failure of gas-bearing coal-rock combination bodies: insights from physical experiments and numerical simulations," *Process Safety and Environmental Protection*, vol. 129, pp. 264–279, 2019.

[40] Q. Lou, X. He, D. Song, Z. Li, A. Wang, and R. Sun, "Time-frequency characteristics of acoustic-electric signals induced by coal fracture under uniaxial compression based on full-waveform," *Journal of Engineering Sciences*, vol. 41, no. 7, pp. 874–881, 2019.

[41] M. Ohnaka and K. Mogi, "Frequency characteristics of acoustic emission in rocks under uniaxial compression and its relation to the fracturing process to failure," *Journal of Geophysical Research - Solid Earth*, vol. 87, no. B5, pp. 3873–3884, 1982.

[42] Z. Li, X. He, L. Dou, G. Wang, D. Song, and Q. Lou, "Bursting failure behavior of coal and response of acoustic and electromagnetic emissions," *Chinese Journal of Rock Mechanics and Engineering*, vol. 38, no. 10, pp. 2057–2068, 2019.

[43] X. Li, S. Chen, S. Wang, M. Zhao, and H. Liu, "Study on in situ stress distribution law of the deep mine: taking Linyi Mining Area as an example," *Advances in Materials Science and Engineering*, vol. 2021, Article ID 5594181, 11 pages, 2021.

[44] Z. Liao, X. Liu, D. Song et al., "Micro-structural damage to coal induced by liquid CO_2 phase change fracturing," *Natural Resources Research*, vol. 30, no. 2, pp. 1613–1627, 2021.

[45] K. Chen, X. Liu, L. Wang, D. Song, B. Nie, and T. Yang, "Influence of sequestered supercritical CO_2 treatment on the pore size distribution of coal across the rank range," *Fuel*, vol. 306, article 121708, 2021.

[46] X. Liu, B. Nie, K. Guo, C. Zhang, Z. Wang, and L. Wang, "Permeability enhancement and porosity change of coal by liquid carbon dioxide phase change fracturing," *Engineering Geology*, vol. 287, article 106106, 2021.

[47] X. Li, S. Chen, S. Liu, and Z. Li, "AE waveform characteristics of rock mass under uniaxial loading based on Hilbert-Huang transform," *Journal of Central South University*, vol. 28, no. 6, pp. 1843–1856, 2021.

[48] H. Wang, J. Ma, G. Wang, H. Gao, G. Cui, and X. Li, "Research on AE source location of linear and plane rock mass," *Shock and Vibration*, vol. 2020, Article ID 8846582, 18 pages, 2020.

[49] N. Li, M. Ge, E. Wang, and S. Zhang, "The influence mechanism and optimization of the sensor network on the MS/AE source location," *Shock and Vibration*, vol. 2020, Article ID 2651214, 16 pages, 2020.